Research Square

Preprints are preliminary reports that have not undergone peer review.
They should not be considered conclusive, used to inform clinical practice,
or referenced by the media as validated information.

Element-based Origin of Magnetism in Nitrogen-Doped Graphene via XAS, XES, and XMCD

Madhuparna Chakraborty

mc559517@ohio.edu

Ohio University

Hirohito Ogasawara

Stanford Synchrotron Radiation Lightsource (SSRL), SLAC National Accelerator Laboratory

Sang-Jun Lee

Stanford Synchrotron Radiation Lightsource (SSRL), SLAC National Accelerator Laboratory

Wojciech M. Jadwisienczak

Ohio University

Article

Keywords: graphene, magnetism, XMCD, XAS, XES, RIXS, graphitic nitrogen

Posted Date: May 18th, 2026

DOI: https://doi.org/10.21203/rs.3.rs-9476915/v1

License: This work is licensed under a Creative Commons Attribution 4.0 International License.
Read Full License

Additional Declarations: No competing interests reported.

Element-based Origin of Magnetism in Nitrogen-Doped Graphene via XAS, XES, and XMCD

Madhuparna Chakraborty[1,2*], Hirohito Ogasawara[3], Sang-Jun Lee[3], and Wojciech M. Jadwisienczak[1,2]

[1]School of Electrical Engineering and Computer Science, Ohio University, Athens, OH 45701, USA

[2]Nanoscale Quantum Phenomena Institute, Ohio University, Athens, Ohio 45701, USA,

[3]Stanford Synchrotron Radiation Lightsource (SSRL), SLAC National Accelerator Laboratory, Menlo Park, CA 94025, USA

[*]mc559517@ohio.edu

Abstract

This work presents an experimental and analytical way to elucidate the origin of magnetism in nitrogen-doped graphene (NG) through advanced synchrotron-based techniques. Here, we use a combination of controlled synthesis and synchrotron-based X-ray absorption spectroscopy (XAS), X-ray emission spectroscopy (XES), and X-ray magnetic circular dichroism (XMCD) to investigate the electronic and magnetic structures of NG. By controlling the thermal parameters of synthesis, we create distinct nitrogen-bonding and defect environments in the NG matrix, enabling us to correlate the chemistry and local magnetism of nitrogen-doped graphene. XAS was used to probe the evolution of unoccupied states and bonding, whereas XES provides additional insight into the occupied electronic states and the chemical environment of the nitrogen species, distinguishing between pyridine-, pyrrole-, and graphite-type bonding. XMCD was used to reveal spin polarization at the carbon and nitrogen K-edges. This study shows that the graphitic nitrogen bonding structure is responsible for the observed magnetization, and thus the magnetic properties of graphene originate intrinsically from the nitrogen-defect-induced electronic structure. Our results connect the scale of C-N bond configurations to the macroscale phenomenon of magnetism and offer a path forward for creating magnetic materials from metal-free carbon. Our approach provides an important platform for studying magnetism in low-dimensional graphene-based systems.

Keywords: graphene, magnetism, XMCD, XAS, XES, RIXS, graphitic nitrogen

Introduction

The magnetism of carbon-based systems has become an important topic in condensed matter physics and materials science, owing to the potential to develop metal-free systems suitable for spintronics and quantum devices[1–4]. Thus, defect- and dopant-induced magnetism in carbon-based materials has emerged as an unconventional route to realizing magnetic order without transition metals. Graphene, a material with excellent electronic properties and light weight, is a very attractive system for achieving magnetism[5]. Unfortunately, it is inherently nonmagnetic. Thus, achieving magnetism while maintaining the electronic structure becomes a challenging task. Various methods have been attempted, but so far, nitrogen (N) doping appears to be one of the most convenient techniques for inducing magnetism in graphene[6,7]. Nitrogen doping creates localized states and alters the electronic structure of graphene[8]. Depending on the bonding, localized states can also give rise to spin-polarized states that lead to ferromagnetism[6–8]. Nitrogen primarily exists in three forms in doped graphene: pyridine, pyrrole, and graphitic configurations, respectively[9,10]. There have been theoretical studies of magnetism observed in such systems, but the microscopic mechanism of magnetism at room temperature remains unclear. On the basis of the results of theoretical studies, the hypothesis is that nitrogen at a graphitic site induces magnetism by polarizing the

π-bonding network of graphene[8,11]. In addition to theoretical studies, element-specific spectroscopic methods such as X-ray absorption spectroscopy (XAS)[12], X-ray emission spectroscopy (XES)[12], and X-ray magnetic circular dichroism (XMCD)[13] can provide an important route toward deepening our understanding of this issue[14]. In XAS, the absorption of energy, normally in the form of a photon, causes excitation of an electron from the core state to an empty state. Thus, XAS probes the empty states. XAS provides direct access to the local electronic structure and chemical bonding in nitrogen-doped graphene (NG) by probing the transitions between the core levels and unoccupied states. Furthermore, XAS at the C and N K-edges in NG can provide sensitive information on the unoccupied electronic states and local bonding environment, enabling the determination of specific N species through the appearance of π^* and σ^*resonances and their interactions with the graphene lattice[15]. Information on the nature of N bonding can be obtained from the analysis of the positions, intensities, and line shapes of the observed features. From this information, the role of N doping in the electronic properties of graphene and its impact on the formation of local magnetism can be determined[16,17]. In contrast, XES enables investigation of the transition of an electron from the upper-occupied state following the decay of an existing core hole, which is necessary for obtaining information on occupied states[18]. With XES, one can gain additional insight into occupied electronic states and the valence-band structure of NG[19]. XES analysis can be used to obtain information on transitions between the occupied and core-hole states, and therefore on the properties of valence electrons, as well as on π and σ states in the carbon-nitrogen lattice, along with the influence of nitrogen incorporation, can be obtained. Together, XAS and XES can provide information on both occupied and unoccupied electronic states in NG system. On the other hand, XMCD offers an element-selective approach to investigate spin polarization in NG. It is defined as the differential X-ray absorption of left circularly polarized (μ^-) and right circularly polarized (μ^+) light in a magnetic field[20,21]. XMCD is particularly sensitive to magnetic moments localized at the atomic and orbital levels. On the C and N K-edges, XMCD detects the spin polarization of the p-orbitals that make up the graphene π-conjugated system. Most importantly, XMCD allows determining whether the observed magnetism arises from intrinsic magnetic ordering or from external factors, such as magnetic impurities[22].

Here, we integrate NG synthesis with XAS, XES, and XMCD studies to elucidate its electronic and magnetic properties at the atomic scale. By fine-tuning the thermal annealing conditions, we can achieve specific nitrogen environments. This strategy allows us to establish a direct correlation between the local chemical environment of the nitrogen configuration and the associated magnetism.

Materials and methods

NG was synthesized using commercially purchased fluorinated graphite (FG) as the starting material. FG was thermally treated in an ammonia atmosphere at 400 °C in a tube furnace for 1 hour to generate sample S1. Sample S1 was subsequently annealed at 600 °C for an hour in an inert atmosphere to generate sample S2. The graphite layers in bulk FG material are weakly held together by van der Waals interactions, which are readily disrupted by the evolved gas in Stage 1, leading to the exfoliation of graphite into graphene[7]. An ammonia atmosphere favors nitrogen doping, whereas annealing in Stage 2 promotes the restructuring of N configurations, producing sample S2.

Magnetic measurements were performed using a vibrating Sample Magnetometer (VSM) as part of a physical properties measurement system (PPMS). The field-dependent magnetization (M-H loop) was measured at room temperature (300 K) up to ±1 T, whereas the temperature-dependent magnetization

was determined from 2-350 K. The diamagnetic background was corrected from each magnetic measurement. Element-specific spectroscopy and magnetic properties have been studied using XAS, XES, and XMCD experiments at the Stanford Linear Accelerator Laboratory (SLAC). Experiments were carried out on beamline 13-2, an elliptically polarizing undulator (EPU) beamline that is optimized for soft X-ray core-level spectroscopy. XAS, XES, and XMCD spectra were collected at the C and N K-edges in total electron yield (TEY) mode. The spectra were measured with high sensitivity with an energy resolution of 1.5 eV in the soft X-ray regime. The beamline covers the energy range of 180–1450 eV with a resolution of $\Delta E/E \sim 10^{-4}$ and a photon flux of $10^{11} - 10^{12}$ photons s^{-1}. All the experiments were performed under ultrahigh vacuum conditions. The collected spectra were normalized to the photon flux, and suitable backgrounds were subtracted to improve sample-to-sample comparison. XMCD spectra were calculated by comparing absorption spectra taken under opposite circular polarizations with a magnetic field applied.

Results and Discussion

The magnetic field-magnetization (M–H) curve provides initial insight into the magnetic response of NG. Figure 1 shows the overall magnetic properties of the NG samples S1 and S2. Figure 1(a), which depicts the magnetization as a function of the applied field (M-H) measurements at 300 K, clearly shows the magnetic response of the samples in the applied field up to ±1 T. In contrast to sample S1, the magnetization in sample S2 is significantly greater, demonstrating that the postsynthesis annealing stage facilitates magnetic ordering by modifying structural defects. Specifically, the coercivity and remanence of sample S2 are 750 Oe and 0.023 emu g^{-1} whereas for sample S1 are 40 Oe and 0.002 emu g^{-1}, respectively, suggesting stronger magnetic interactions and better spin-polarization stabilization after Stage 2. This improvement in S2 results from thermal changes in the defect environment and in nitrogen bonding. The temperature-dependent magnetization (M-T) data obtained under a magnetic field of 100 Oe (see Figure 1(b)) show the effect of the temperature on the magnetic properties of the samples. In both cases, the magnetization varies continuously with temperature, indicating the presence of local magnetic moments rather than long-range magnetic ordering. Specifically, sample S2 shows a stronger temperature dependence of the magnetization than does sample S1.

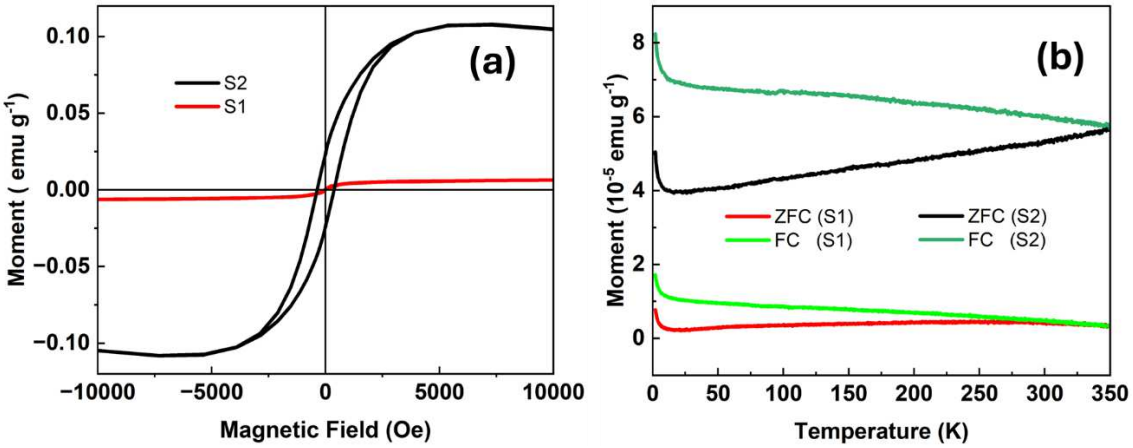


Fig.1 (a) Magnetization as a function of the applied magnetic field (M–H) for NG samples S1 and S2 measured at 300 K over a field range of ±1 T. (b) Temperature-dependent magnetization (M–T) for NG samples S1 and S2 measured under an applied field of 100 Oe.

To gain deeper insight into the electronic structure and the local bonding environment of individual atoms, XAS was performed. The absorption edges of a material are element-specific, and there is a sudden increase in the absorption coefficient when a core-level electron is excited to the unoccupied orbitals or in an unbound state. The K-edge arises from the excitation of a core 1s electron to unoccupied electronic states above the Fermi level. To further elucidate the local electronic structure and bonding environment, XAS measurements at the N K-edge and C K-edge were performed on both the S1 and post-annealed, S2 NG samples. The N K-edge spectra of NG before and after annealing are shown in Figure 2(a). Both samples S1 and S2 in Figure 2(a) show three clear peaks in the π^* region. The peak seen around 397.3 eV matches the typical pattern of pyridinic N in the N 1s core-level spectrum. A peak appears at approximately 398.2 eV, which is due to the presence of pyrrolic N in the structure. The peak observed at 399.8eV shows that there is graphitic N in the graphene structure[6,7]. The growth of peaks higher than 404.5 eV can be linked to the σ^* resonance[23]. The ratio of pyrrolic-to-pyridinic is 0.988, and that of graphitic-to-pyridinic is 0.968 in sample S1, respectively, whereas in sample S2, their ratios have increased to 1.002 and 0.99. This represents an increase of about 1.4% for pyrrolic nitrogen and 2.3% for graphitic N. This shows that annealing promotes graphitic N configuration. Increasing the NG processing temperature favors the pyridinic N configuration over the pyrrolic and graphitic configurations[24]. The increased graphitic N indicates greater substitution of carbon atoms within the hexagonal lattice, resulting in nitrogen atoms being coordinated with three neighboring sp^2 carbon atoms. The relationship between the electronic structure and the material's magnetism is evident from the combination of XAS (see Figure 2) and M-H data (see Figure 1). XAS spectra taken at the N K-edge show a significant increase in the contribution from peaks corresponding to graphitic N, which can affect electron delocalization and cause spin polarization. This is corroborated by the observation that M-H plots (Figure 1(a)) show higher magnetization, coercivity, and remanence in sample S2 than in sample S1.

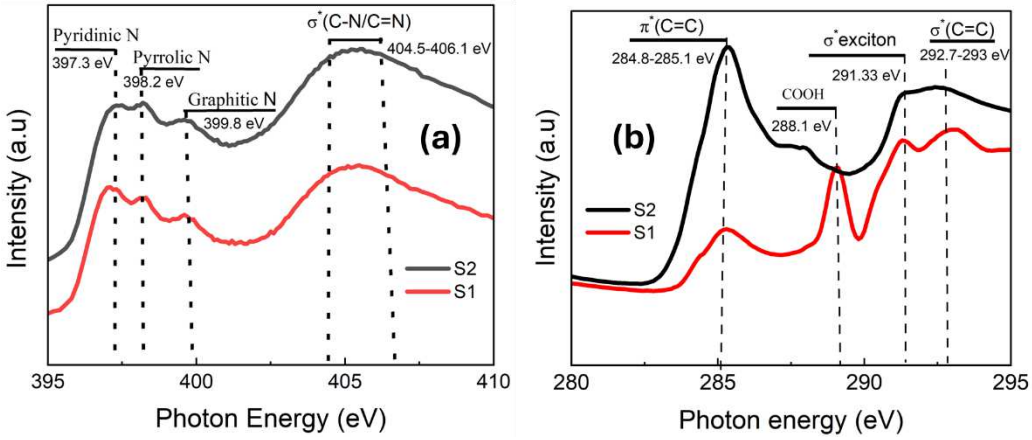


Fig.2 (a) XAS spectra of (a) N K-edge and (b) C K-edge for samples S1 and S2, highlighting the evolution of electronic structure and bonding environments upon thermal treatment.

The C K-edge spectra of the NG after annealing in different stages are shown in Figure 2(b). A clear peak seen at ~285 eV matches the anticipated movement of electrons from the C 1s level to the π* orbital. The peak becomes sharper after stage 2, indicating more graphitization of the NG system.

A double peak in resonance seen at ~292 eV, is related to the C 1s $\rightarrow \sigma^*$ transition. This mainly comes from two sources, one is the excitonic contribution around 291.33 eV, and the other is a band-like contribution at 292.7 eV[25,26]. The presence of a carboxyl component at ~288.1 eV indicates surface oxidation, with carbon in a higher oxidation state (+2 or +3). For the S2 sample, the peak at 288.1 eV decreases considerably; instead, a peak occurs in the S2 spectrum that happens between the π^* and σ^* resonance, in the energy range between 286 and 288 eV, which is called the fingerprint region[27]. This arises due to structural defects and chemical changes in graphene[27,28]. It is reasonable to assume that the appearance of the peak in S2 sample could be due to defects forming in graphene and/or nitrogen incorporation to defect sites[28].

To test the assumption that magnetic ordering in NG is dominated by the nitrogen-doping configuration, we performed XMCD because this technique investigates the magnetic characteristics of materials at the atomic level. Thus, XMCD serves as a direct probe of spin and orbital magnetic moments.

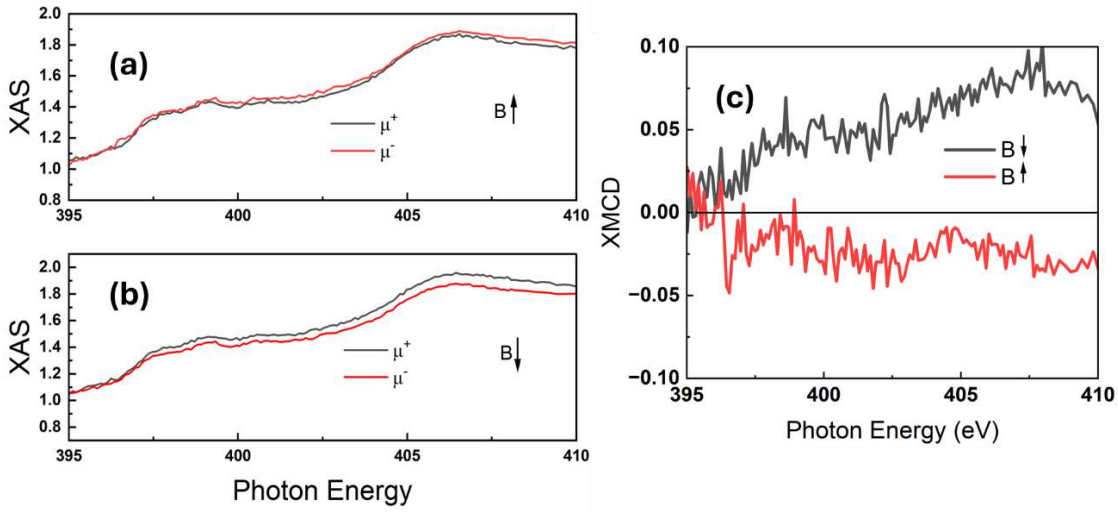


Fig.3 Representative XAS and XMCD spectra measured as a function of photon energy at the N K-edge (a) XAS recorded with opposite circular polarizations (μ^+ and μ^-) under an externally applied magnetic field (B↑). (b) XAS recorded with opposite circular polarizations (μ^+ and μ^-) under an external magnetic field applied (B↓). (c) Corresponding XMCD spectra obtained from the difference between μ^+ and μ^- for opposite magnetic field directions (B↑ and B↓).

The XMCD spectrum was derived by subtracting the XAS spectra, corresponding to the magnetic fields applied parallel and antiparallel to the photon helicity of the incident light, which is equivalent to the difference between the right-handed (μ^+) and left-handed circularly polarized light spectra (μ^-) recorded in a fixed magnetic field in Figures 3(a) and (b). The peaks in the XMCD spectrum matched the multiplet structures of the XAS spectra. The spectral signatures around the major absorption feature (~401-408 eV) suggest that these states have a nonzero magnetic dipole moment. The related XMCD, defined as $\mu^+ - \mu^-$, is displayed for both field polarizations in Figure 3(c). As expected, the XMCD feature reverses sign under field reversal, thereby confirming the magnetic nature of the effect. The spectral signature displays distinct signs of spin-orbital-polarized states, namely, a strong positive peak when B↓ and a corresponding

negative peak when B↑[29]. Therefore, the sizeable XMCD response demonstrates that nitrogen exhibits intrinsic spin polarization and is a primary source of magnetism in the sample.

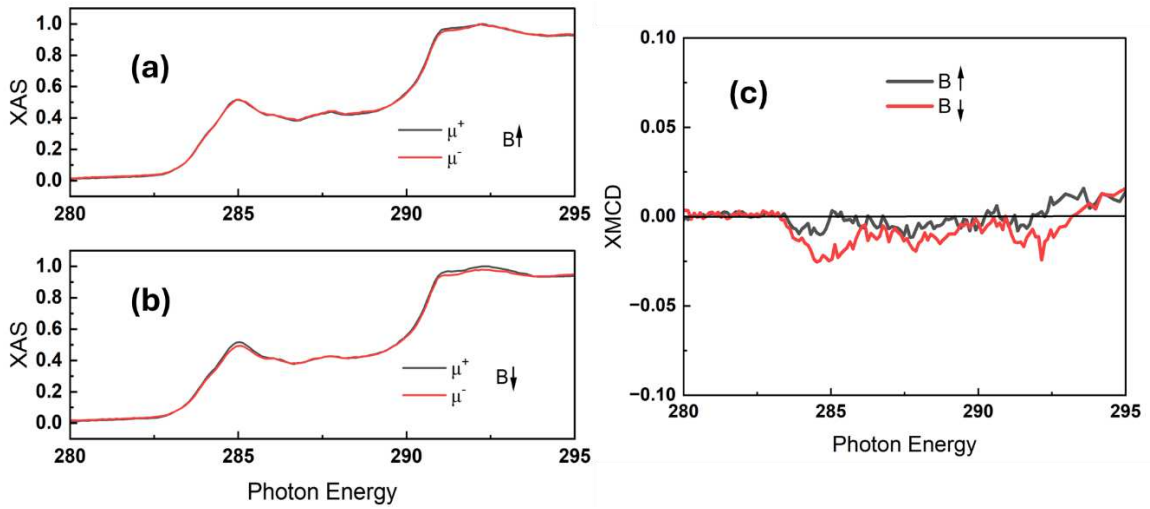


Fig. 4 Representative XAS and XMCD spectra measured as a function of photon energy at the C K-edge. (a) XAS recorded with opposite circular polarizations (μ^+ and μ^-) under an external magnetic field applied upward (B↑). (b) XAS recorded with opposite circular polarizations (μ^+ and μ^-) under an external magnetic field applied downward (B↓). (c) Corresponding XMCD spectra obtained from the difference between μ^+ and μ^- for opposite magnetic field directions (B↑ and B↓).

Figure 4(a) and (b) show the helicity-dependent XAS spectra under opposite magnetic fields at the C K-edge. The absorption peaks exhibit the expected features of C K-edge spectra, with a prominent pre-edge peak at about 285 eV due to π^* levels and a broader σ^* resonance around 290 eV. The comparable intensity values for the μ^+ and μ^- scans suggest no polarization asymmetry. The XMCD is weak, remaining below ~0.02 on a normalized scale, and no prominent dichroism is observed at higher energies, suggesting a non-magnetic nature of the σ^* levels. Taken together, the N and C K-edge results clearly establish that the magnetism in NG is centered at the nitrogen dopant sites. It also reiterates that it is intrinsic to the NG material, not due to magnetic contamination. These results establish nitrogen defect-induced π-electron magnetism as the microscopic origin of the magnetic behavior observed in this system.

Resonant inelastic x-ray scattering (RIXS) is a powerful, element-specific technique that probes the electronic structure of materials by using photons both as the probe and the detector, with the energy of the incoming photons tuned to an absorption edge to excite electrons to unoccupied states. Following relaxation from the excited state to ground state through emission of another photon, RIXS allows one to probe different excitations in the material, including crystal-field excitations and charge transfer excitations, by using the energy difference between the incoming and outgoing photons[30,31]. Figure 5 shows two-dimensional RIXS intensity maps as a function of emission energy and excitation energy for samples S1 and S2. We selectively observe the occupied electronic states projected on the nitrogen atom. Whereas projecting RIXS along the emission energy axis of Figures 5(a) and (e) is equivalent to conventional XES, which

highlights occupied states, projecting RIXS along the excitation energy axis of Figures 5(a) and (e) is equivalent to conventional XAS. RIXS can generate site-selective XES by matching the excitation photon energy to the XAS peak energy of different atomic sites, which distinguishes electronic structures between chemically inequivalent sites of the same element[32]. Figure 5 also shows XES plotted against the binding energy scale of (b) pyridinic, (c) pyrrolic, and (d) graphitic N in S1 and (f) pyridinic, (g) pyrrolic, and (h) graphitic N in S2. Based on dipole approximation rules, XES provides information about partial density of nitrogen $2p$ states where the $2p$ orbitals of nitrogen are spin polarized and play a key role in observed magnetism. Also, the binding energy of the intense peak corresponds to that of nitrogen p states, which are clearly different between pyridinic, pyrrolic, and graphitic nitrogen sites.

In general, NG systems containing pyridinic, pyrrolic, and graphitic N can be distinguished by specific shifts in their energy levels, replicating their unique bonding environments. Specifically, pyridinic N sits at the edges or vacancies and contributes two electrons to σ sigma bonds, while nitrogen in a graphitic setting replaces a carbon atom within the hexagonal lattice and contributes to the delocalized π system[33].

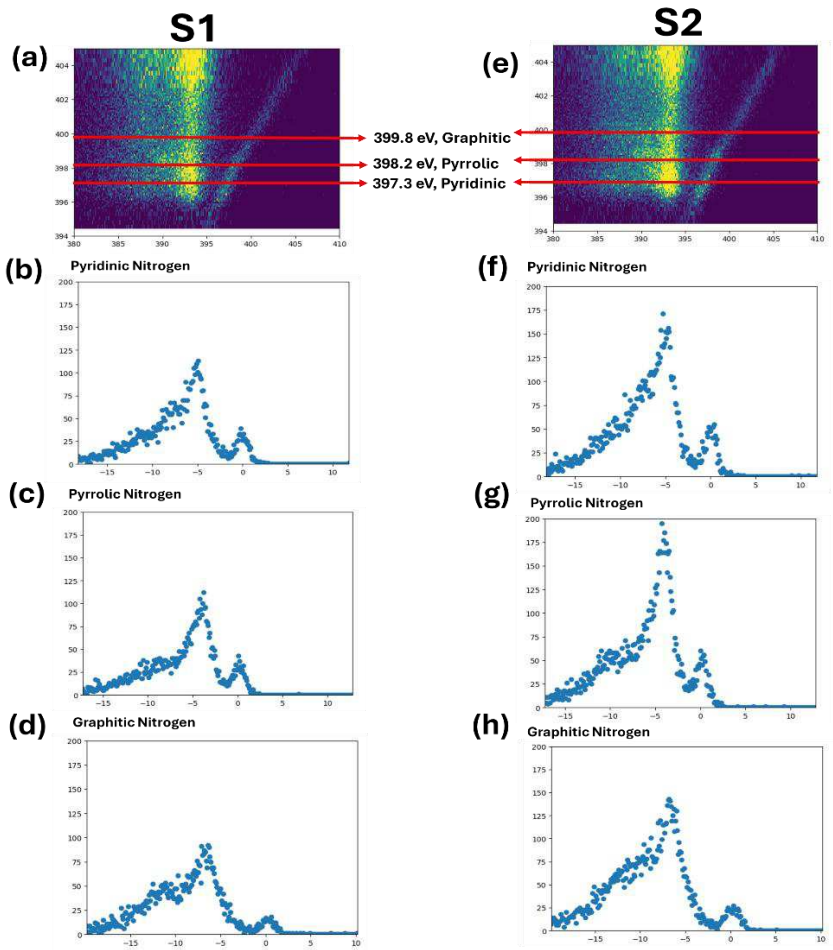


Fig.5 N K-edge XES analysis of nitrogen-doped graphene samples from RIXS. (a, e) Two-dimensional RIXS intensity maps as a function of emission energy (Y-axes) and excitation energy (X-axes) for samples S1 and S2. (c–h) site-selective XES projections showing pyridinic, pyrrolic, and graphitic N contributions for samples S1 and S2. The emission energy is shifted using the N1s XPS binding energy.

Therefore, in studied NG material, the incorporation of nitrogen in non-uniform bonding configurations locally breaks sublattice symmetry and generates spatially distributed magnetic moments. Owing to the intrinsic disorder of dopant placement and the competition between ferromagnetic and antiferromagnetic exchange interactions mediated by the graphene π-electron network, these moments do not readily establish long-range ferromagnetic order. Instead, the system naturally evolves toward a less-ordered spin configuration (e.g. spin glass-like state), where frozen and fluctuating spin clusters coexist and collectively give rise to measurable magnetization. Therefore, RIXS and XMCD complement each other by combining bulk-sensitive, elementary excitation mapping with element-specific, quantitative ground-state magnetic moment analysis, which confirms the nitrogen site being responsible for imparting magnetism.

Conclusions

In summary, this study demonstrates an explicit correlation between the electronic structure and magnetic properties of nitrogen-doped graphene via a controlled experimental approach that combines bulk magnetization measurements with element-specific synchrotron radiation techniques. The results of X-ray absorption spectroscopy revealed a gradual change in the local environment due to thermal annealing of the initial fluorinated graphite, which is converted to nitridated graphene during the two-stage process, whereas X-ray magnetic circular dichroism indicates clear spin-polarization behavior in the carbon-nitrogen lattice. By correlating spectroscopic fingerprints with magnetic properties, we confirm that magnetism arises inherently from electronic effects associated with defects induced by nitrogen doping, not from extrinsic impurities themself. The study reveals that nitrogen introduction and the subsequent formation of defect levels play an important role in the development of local magnetic moments and their interplay. From a broader perspective, this research provides a reliable approach to exploring and manipulating magnetism in two-dimensional carbon-based non-metallic materials. Through the manipulation of magnetic properties via doping and annealing, new opportunities arise for developing novel spintronics and quantum devices based on carbon allotropes.

References

1. Popov, V. V., Orlova, T. S., Spitsyn, A. A., Kirilenko, D. A. & Dyakonov, K. V. Magnetic carbon-nanoparticles behavior of biomorphic pyrolytic carbons. *J. Magn. Magn. Mater.* **640**, 173811 (2026).
2. Ranade, V., Gautam, S. & Chae, K. H. Magnetism in carbon-based fiber materials. *J. Magn. Magn. Mater.* **586**, 171210 (2023).
3. Pawar, S., Duadi, H. & Fixler, D. Recent Advances in the Spintronic Application of Carbon-Based Nanomaterials. *Nanomaterials* **13**, 598 (2023).
4. Li, R. *et al.* Research of Low-Dimensional Carbon-Based Magnetic Materials. *ACS Appl. Electron. Mater.* **4**, 3263–3277 (2022).
5. Geha, A. G., aguado, Y. & Nadiaye, M. B. Graphene, a material with exceptional electronic properties. Preprint at https://doi.org/10.48550/ARXIV.2402.00599 (2024).
6. Chakraborty, M., Jensen, G., Ingram, D. C., Stinaff, E. & Jadwisienczak, W. M. Magnetic Properties of Nitrogen-Doped Graphene Induced by Dopant Configurations. *Nanomaterials* **15**, 1694 (2025).
7. Chakraborty, M. *et al.* Converting Fluorinated Graphite to Nitridated Graphene for Room-Temperature Magnetic Applications. *J. Electron. Mater.* https://doi.org/10.1007/s11664-025-12632-w (2026).

8. Babar, R. & Kabir, M. Ferromagnetism in nitrogen-doped graphene. *Phys. Rev. B* **99**, 115442 (2019).
9. Solati, N. *et al.* Pyridinic nitrogen induced compressed bilayer graphene for oxygen reduction reaction. *Mater. Today Energy* **35**, 101323 (2023).
10. Yutomo, E. B., Noor, F. A. & Winata, T. Effect of the number of nitrogen dopants on the electronic and magnetic properties of graphitic and pyridinic N-doped graphene – a density-functional study. *RSC Adv.* **11**, 18371–18380 (2021).
11. Błoński, P. *et al.* Doping with Graphitic Nitrogen Triggers Ferromagnetism in Graphene. *J. Am. Chem. Soc.* **139**, 3171–3180 (2017).
12. *X-Ray Absorption and X-Ray Emission Spectroscopy: Theory and Applications*. (Wiley, 2016). doi:10.1002/9781118844243.
13. Stöhr, J., Padmore, H. A., Anders, S., Stammler, T. & Scheinfein, M. R. Principles of X-Ray Magnetic Dichroism Spectromicroscopy. *Surf. Rev. Lett.* **05**, 1297–1308 (1998).
14. Iglesias-Juez, A., Chiarello, G. L., Patience, G. S. & Guerrero-Pérez, M. O. Experimental methods in chemical engineering: X -ray absorption spectroscopy— XAS , XANES , EXAFS. *Can. J. Chem. Eng.* **100**, 3–22 (2022).
15. Hellgren, N. *et al.* Electronic structure of carbon nitride thin films studied by X-ray spectroscopy techniques. *Thin Solid Films* **471**, 19–34 (2005).
16. Sterling, C. M. *et al.* Sensitivity of Nitrogen K-Edge X-ray Absorption to Halide Substitution and Thermal Fluctuations in Methylammonium Lead-Halide Perovskites. *J. Phys. Chem. C* **125**, 8360–8368 (2021).
17. Zimmermann, P. *et al.* Modern X-ray spectroscopy: XAS and XES in the laboratory. *Coord. Chem. Rev.* **423**, 213466 (2020).
18. Wang, J. *et al.* In situ X-ray spectroscopies beyond conventional X-ray absorption spectroscopy on deciphering dynamic configuration of electrocatalysts. *Nat. Commun.* **14**, 6576 (2023).
19. Lee, K. J., Chang, S. H. & Kim, J. Mapping Resonant Inelastic X-ray Scattering Onto Electronic Structure of Iridium Compounds, Rapid Research Letters **20**, e202500463 (2026).
20. Van Der Laan, G. & Figueroa, A. I. X-ray magnetic circular dichroism—A versatile tool to study magnetism. *Coord. Chem. Rev.* **277–278**, 95–129 (2014).
21. Fujiwara, A., Asakura, K., Harada, I., Ogasawara, H. & Kotani, A. XMCD Study on Electronic and Magnetic States of RareEarth 5d Electrons in Laves Compounds, RFe2 R RareEarth. *Phys. Scr.* **113** (2005)115a00113.
22. Gambardella, P. *et al.* Localized Magnetic States of Fe, Co, and Ni Impurities on Alkali Metal Films. *Phys. Rev. Lett.* **88**, 047202 (2002).
23. Usachov, D. *et al.* Nitrogen-Doped Graphene: Efficient Growth, Structure, and Electronic Properties. *Nano Lett.* **11**, 5401–5407 (2011).
24. Wu, S. *et al.* Pyridinic- and Pyrrolic Nitrogen in Pyrogenic Carbon Improves Electron Shuttling during Microbial Fe(III) Reduction. *ACS Earth Space Chem.* **5**, 900–909 (2021).
25. Lee, V. *et al.* Soft X-ray Absorption Spectroscopy Studies of the Electronic Structure Recovery of Graphene Oxide upon Chemical Defunctionalization. *J. Phys. Chem. C* **116**, 20591–20599 (2012).
26. Fischer, D. A., Wentzcovitch, R. M., Carr, R. G., Continenza, A. & Freeman, A. J. Graphitic interlayer states: A carbon *K* near-edge x-ray-absorption fine-structure study. *Phys. Rev. B* **44**, 1427–1429 (1991).

27. Ehlert, C., Unger, W. E. S. & Saalfrank, P. C K-edge NEXAFS spectra of graphene with physical and chemical defects: a study based on density functional theory. *Phys Chem Chem Phys* **16**, 14083–14095 (2014).
28. M. Santhosh, N. *et al.* N-Graphene Nanowalls via Plasma Nitrogen Incorporation and Substitution: The Experimental Evidence. *Nano-Micro Lett.* **12**, 53 (2020).
29. Junghoefer, T. *et al.* Magnetic behavior in metal-free radical thin films. *Chem* **8**, 801–814 (2022).
30. Kühn, T.-J., Hormes, J., Matoussevitch, N., Bönnemann, H. & Glatzel, P. Site-Selective High-Resolution X-ray Absorption Spectroscopy and High-Resolution X-ray Emission Spectroscopy of Cobalt Nanoparticles. *Inorg. Chem.* **53**, 8367–8375 (2014).
31. Miyawaki, J., Yamamoto, K., Kiuchi, H. & Harada, Y. Ultrahigh Resolution and High Efficiency RIXS/XES Spectrometers at NanoTerasu BL02U and BL07U. *Synchrotron Radiat. News* **38**, 4–12 (2025).
32. Nilsson, A. & Pettersson, L. G. M. Chemical bonding on surfaces probed by X-ray emission spectroscopy and density functional theory. *Surf. Sci. Rep.* **55**, 49–167 (2004).
33. Lazar, P., Mach, R. & Otyepka, M. Spectroscopic Fingerprints of Graphitic, Pyrrolic, Pyridinic, and Chemisorbed Nitrogen in N-Doped Graphene. *J. Phys. Chem. C* **123**, 10695–10702 (2019).

Acknowledgements
This work was supported by the Appalachian Semiconductor Education and Technical (ASCENT) Ecosystem Fellowship, sponsored by Intel Inc., and by NSF Major Research Instrumentation Grant No. 2018520. WJ would like to acknowledge support from the NSF Major Research Instrumentation Grant No. 2018520. The use of the Stanford Synchrotron Radiation Lightsource, SLAC National Accelerator Laboratory, is supported by the U.S. Department of Energy, Office of Science, Office of Basic Energy Sciences under Contract No. DE-AC02-76SF00515.
Funding
This research was funded by the Ohio University Student Enhancement Award, the Nanoscale & Quantum Phenomena Institute (NQPI) Fellowship, and the EECS Department at Ohio University through the iSURF project.
Author contributions
Author Contributions: Conceptualization, M.C., W.M.J. and H.O.; Methodology, M.C., W.M.J., H.O. and S-J.L; Validation, W.M.J. and H.O; Formal analysis, M.C., W.M.J., H.O. and S-J.L; Investigation, M.C., H.O. and S-J.L; Resources, M.C., W.M.J., H.O. and S-J.L.; Data curation, M.C. H.O; Writing—original draft, M.C.; Writing—review & editing, M.C., W.M.J., H.O.; Supervision, W.M.J. and H.O; Project administration, W.M.J. and H.O.; Funding acquisition, W.M.J. and H.O. All authors have read and agreed to the published version of the manuscript.
Data availability statement
Data supporting the findings is contained within the article and is available from the corresponding author on reasonable request.